Computational Condensed Matter 3 (2015) 21–29

Contents lists available at ScienceDirect

Computational Condensed Matter

journal homepage: http://ees.elsevier.com/cocom/default.asp

Regular article

Theoretical study of adsorption of CO gas on pristine and AsGa-doped (4, 4) armchair models of BPNTs

Mahdi Rezaei-Sameti*, Sahar Yaghoobi

Department of Applied Chemistry, Faculty of Science, Malayer University, Malayer, 65174, Iran

ARTICLE INFO

Article history:
Received 14 September 2014
Received in revised form
29 December 2014
Accepted 13 January 2015
Available online 14 January 2015

Keywords:
BPNTs
Adsorption CO
DFT
AsGa-doped
NMR and NQR

ABSTRACT

In this research, we investigate and discuss the adsorption of carbon monoxide gas (CO) on the outside and inside surface of pristine and AsGa doped of (4, 4) armchair boron phosphide nanotubes (BPNTs). The structural, electrical parameters, NMR, NQR parameters and chemical reactivity of these compounds were compared using DFT-based descriptors such as global hardness, global softness, electrophilicity, electronic chemical potential, and electronegativity. The considerable changes in the adsorption energies, energy gap values, global hardness, and NMR parameters generated by doping AsGa and orientation of CO adsorption and show the high sensitivity of the electronic properties of BPNTs towards the adsorption of CO on its surface. The results of the adsorption energy suggest that the AsGa decorated BPNTs are good candidate for CO adsorption. The NMR and NQR parameters variations in the complex show a significant change in the presence of CO adsorption and AsGa-doped. The quantum molecular descriptors and molecular orbital energies of the complex show that the nanotube can absorb CO molecule in its pristine and AsGa-doped form, and that the AsGa-doped and adsorption on the outside surface of nanotube is more favorable than pristine model and inside surface.

1. Introduction

In the past decades, the significant research efforts have been done to monitoring and control of air pollutions [1–3]. Air pollutions come from both natural and human-made (anthropogenic) sources. However, globally human-made pollutants from combustion, construction, mining, agriculture and warfare are increasingly significant in the air pollution equation [4–6]. Therefore, much research has been focused on the development of suitable gas sensitive materials for continuous monitoring and setting off alarms for hazardous chemical vapors present beyond specified levels [7–10]. Carbon monoxide, a colorless, odorless, highly toxic gas is one of the most common and widely distributed air pollutants. It arises from the incomplete burning of materials, natural gas, industrial processes, sewage leaking and biological decay [11–16]. Recently, numerous efforts have been focused on investigating the nanotube materials as gas adsorbents and sensitive methods for detecting CO [17–21]. Recent investigations reveal that, pure nanotubes cannot be used for detection of CO molecules because CO cannot be adsorbed completely on their surfaces. Therefore, experimental and theoretical investigations have focused on improving the sensing performance of such pristine tubes toward various gas molecules by doping or functionalizing [22–25]. Following our previous works on the study of NMR and structural parameters of AsGa, Ga, C doped on BPNTs [26–29]. In the current research, DFT calculations are performed to elucidate the relationship between the electronic structures of pristine, AsGa-doped BPNTs and the adsorption of carbon monoxide molecule at different positions of outside and inside BPNTs, in order to reveal some clues for chemical sensor design. For this aim, at first step all structures of nanotube/CO complex at different configurations have been optimized, and then, the electronic structure properties, quantum parameters, adsorption energies, band gaps, HOMO and LUMO orbitals, NQR and NMR parameters of all models of BPNTs are investigated.

2. Computational methods

In this work, the representative models of (4, 4) armchair single-walled BPNTs in which the ends of the nanotubes are saturated by hydrogen atoms (see Figs. 1 and 2). In the first step, the structures were allowed to relax by all atomic geometrical parameters in the

* Corresponding author.
E-mail addresses: mrsameti@gmail.com, mrsameti@malayeru.ac.ir (M. Rezaei-Sameti).

http://dx.doi.org/10.1016/j.cocom.2015.01.001

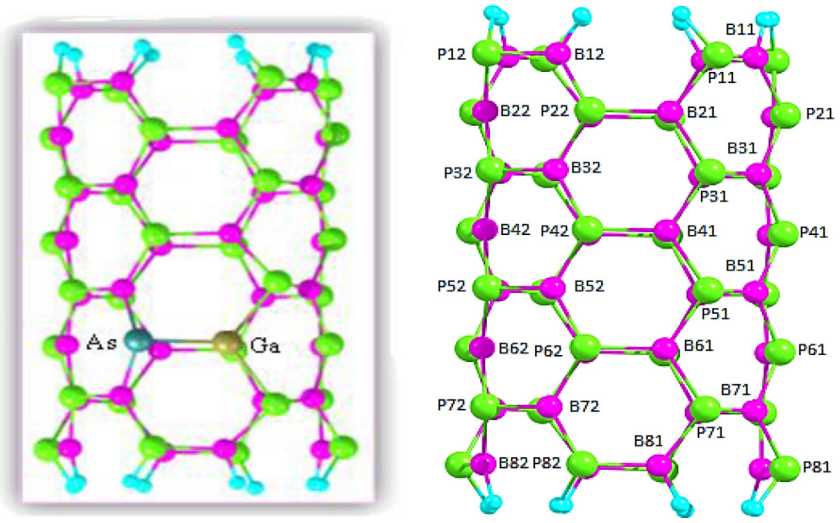

Fig. 1. 2D views of pristine and AsGa-doped of (4, 4) armchair model of BPNTs.

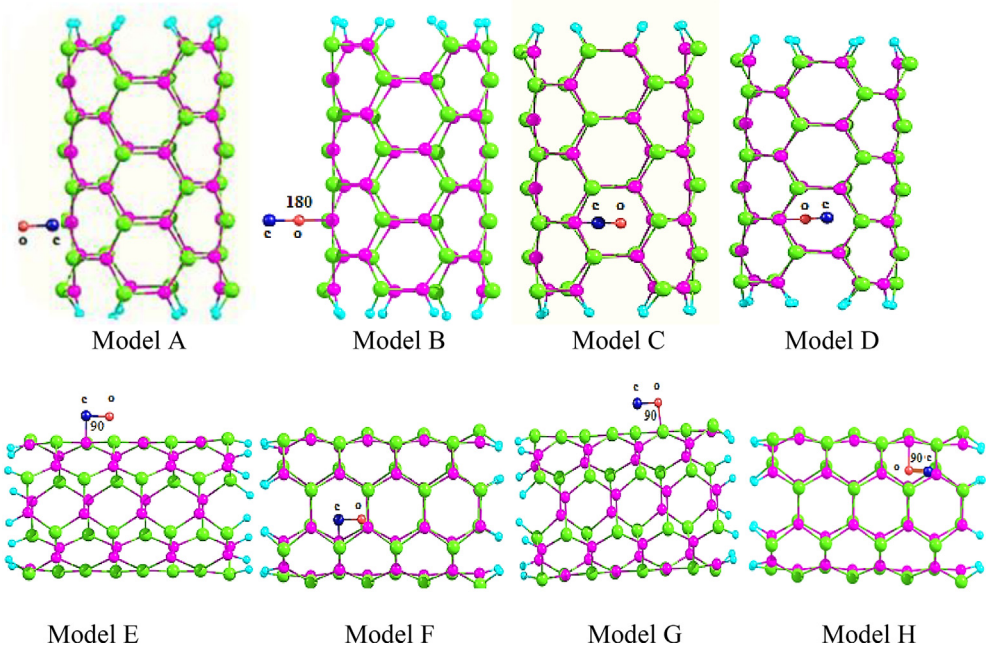

Fig. 2. 2D views of CO adsorption on the outer and inner surface of (4, 4) armchair model of BPNTs, for (A–H) models.

optimization at the DFT level of B3LYP exchange functional and 6-31G (d) standard basis set using the Gaussian 03 set of programs [30]. Subsequently, the CS tensors are calculated in the optimized structures using the same level of the theory. Furthermore, the chemical shielding (CS) tensors at the sites of ^{11}B, ^{31}P nuclei are calculated based on the gauge included atomic orbital (GIAO) approach [31]. The calculated CS tensors in the principal axes system (PAS) ($\sigma_{33} > \sigma_{22} > \sigma_{11}$) are converted to measurable NMR parameters, chemical shielding isotropic (CSI) and chemical shielding anisotropic (CSA) by using Equations (1) and (2), respectively [26–29].

$$CSI(ppm) = \frac{1}{3}(\sigma_{11} + \sigma_{22} + \sigma_{33}) \quad (1)$$

$$CSA(ppm) = \sigma_{33} - (\sigma_{22} + \sigma_{33})/2 \quad (2)$$

Adsorption energy (E_{ads}) of carbon monoxide (CO) on the pristine and AsGa-doped BPNTs was calculated as follows:

$$E_{ads} = E_{BPNTs-CO} - (E_{BPNTs} + E_{CO}) + BSSE \quad (3)$$

Where $E_{BPNTs\text{-}CO}$ was obtained from the scan of the potential energy of the BPNTs–CO, E_{BPNTs} is the energy of the optimized BPNTs structure, and E_{CO} is the energy of an optimized CO and BSSE is a base set superposition errors. The quantum molecular descriptors electronic, chemical potential (μ), global hardness (η), electrophilicity index (ω), energy gap, global softness (S), and electronegativity (χ) of the nanotubes were calculated as follows:

Table 1
Structures parameters of CO adsorption on pristine and AsGa-doped of (4, 4) armchair models of BNNTs, (I) values for pristine and (II) values for AsGa-doped of (A-H) models of adsorption. (See Figs. 1 and 2).

Property	Un adsorbed		Model(A)		Model(B)		Model(C)		Model(D)		Model(E)		Model(F)		Model(G)		Model(H)	
	(I)	(II)	(I)	(II)	(I)	(II)	(I)	(II)	(I)	(II)	(I)	(II)	(I)	(II)	(I)	(II)	(I)	(II)
Bond length																		
P51-B61/Ga	1.89	2.25	2.00	2.27	1.89	2.27	1.89	2.26	1.89	2.27	1.98	2.25	1.98	2.25	1.89	2.25	1.89	2.25
B61/Ga-P62/As	1.88	2.33	1.97	2.35	1.88	2.35	1.88	2.34	1.88	2.35	2.01	2.33	2.01	2.33	1.89	2.34	1.89	2.33
P62/As-B52	1.89	2.02	1.87	2.01	1.89	2.01	1.89	2.01	1.89	2.02	1.93	2.02	1.93	2.02	1.89	2.02	1.89	2.02
P52-B62	1.89	1.89	1.90	1.89	1.89	1.89	1.89	1.89	1.89	1.89	1.89	1.89	1.89	1.89	1.89	1.89	1.89	1.89
P62/As-B72	1.90	2.02	1.87	2.01	1.90	2.01	1.90	2.01	1.90	2.02	1.93	2.02	1.93	2.02	1.90	2.02	1.90	2.02
B72–P72	1.89	1.88	1.90	1.87	1.89	1.87	1.89	1.87	1.89	1.88	1.88	1.88	1.88	1.88	1.89	1.88	1.89	1.88
B72-P82	1.90	1.92	1.90	1.93	1.90	1.93	1.90	1.93	1.90	1.92	1.91	1.92	1.91	1.92	1.90	1.92	1.90	1.92
B61/Ga-P71	1.90	2.26	2.01	2.28	1.90	2.28	1.90	2.26	1.90	2.28	1.98	2.26	1.98	2.26	1.90	2.26	1.90	2.26
P71-B71	1.89	1.91	1.90	1.91	1.89	1.91	1.89	1.91	1.89	1.91	1.90	1.91	1.90	1.91	1.89	1.92	1.89	1.91
Bond angle																		
B61/Ga-P62/As-B52	111	93	117	95	111	95	111	94	111	93	101	90	101	94	111	93	111	94
B41-P51-B61/Ga	117	108	111	109	117	109	117	108	117	108	113	107	113	108	117	108	116	108
P51-B61/Ga-P62/As	121	122	113	122	122	122	121	122	121	122	116	119	116	122	121	122	122	121
B81-P71-B61/Ga	115	104	108	105	115	105	115	105	114	105	111	102	111	104	114	103	115	103
P71-B61/Ga-P62/As	121	123	112	124	121	124	121	124	121	124	116	120	116	123	121	124	121	124
B61/Ga-P62/As-B72	112	93	117	94	112	94	112	93	112	93	102	90	102	94	112	93	112	93
B61/Ga-P71-B71	111	102	108	105	111	105	111	103	111	103	104	99	104	102	111	102	112	102
B51-P51-B61/Ga	111	102	108	105	111	104	110	103	110	102	102	99	102	102	111	102	111	102
P51-B61/Ga-P71	117	113	114	114	117	114	117	114	117	114	109	109	109	113	117	113	117	113

$$\mu = -(I + A)/2 \tag{4}$$

$$\eta = (I - A)/2 \tag{5}$$

$$\chi = -\mu \tag{6}$$

$$\omega = \mu^2 \big/ 2\eta \tag{7}$$

$$S = 1/2\eta \tag{8}$$

$$Energy\ gap = E_{LUMO} - E_{HOMO} \tag{9}$$

Where I ($-E_{HOMO}$) is the ionization potential and A ($-E_{LUMO}$) the electron affinity of the molecule. The electrophilicity index is a measure of the electrophilicity power of a molecule [32–36,39–44]. The NQR parameters (C_Q, η_Q) are determined as above the level of theory. The NQR parameters refer to the interaction energy of the nuclear electric quadrupole moment and the EFG tensors at the site of quadrupole nucleus. Equations (10) and (11) used to convert the EFG tensors to the measurable parameters C_Q and η_Q [37]. The standard Q value of B atom is 40.59 *mb* [38].

$$C_Q(MHZ) = e^2 Q q_{zz} h^{-1} \tag{10}$$

$$\eta_Q = \left|\left(q_{xx} - q_{yy}\right)\big/ q_{zz}\right| \quad \left(q_{zz} > q_{yy} > q_{xx}\right) \quad 0 < \eta_Q < 1 \tag{11}$$

Table 2
Adsorption energy and base set superposition error for (A-H) models of CO adsorption on pristine and AsGa-doped of BPNTs.

Species	E_{ads} (eV)	E_{ad} (kcal/mol)	BSSE (kcal/mol)	$E_{ads\text{-}BSSE}$ (kcal/mol)	R(B/Ga_CO)
Undoped					
Model (A)	−0.193	−4.453	0.007	−4.446	1.53
Model (B)	−0.025	−0.596	0.001	−0.594	3.99
Model (C)	−0.024	−0.556	0.001	−0.555	3.06
Model (D)	−0.029	−0.668	0.001	−0.667	3.68
Model (E)	0.066	1.532	0.008	1.541	1.54
Model (F)	0.065	1.519	0.008	1.528	1.54
Model (G)	0.086	1.993	0.006	1.999	3.65
Model (H)	0.098	2.272	0.006	2.278	3.94
AsGa-doped					
Model (A)	−0.303	−7.003	0.012	−6.990	2.08
Model (B)	−0.303	−7.002	0.012	−6.990	2.08
Model (C)	−0.181	−4.183	0.008	−4.175	2.99
Model (D)	−0.183	−4.238	0.008	−4.229	3.21
Model (E)	−0.183	−4.224	0.016	−4.207	2.82
Model (F)	−0.032	−0.746	0.011	−0.735	3.80
Model (G)	−0.049	−1.133	0.011	−1.122	2.68
Model (H)	−0.028	−0.653	0.011	−0.641	3.60

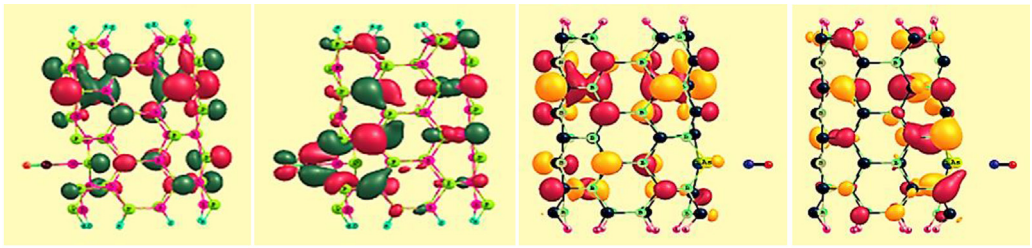

(I) (II) (III) (IV)

Model A

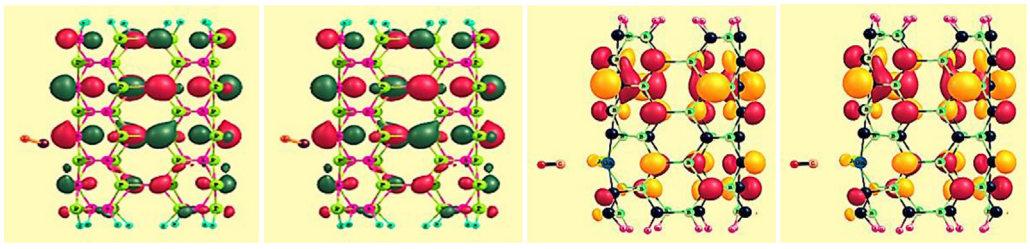

(I) (II) (III) (IV)

Model B

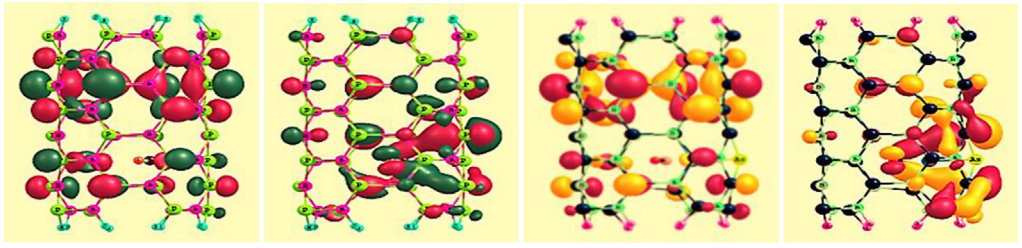

(I) (II) (III) (IV)

Model C

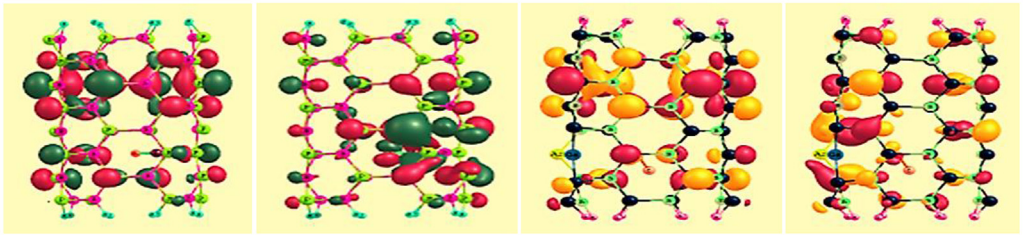

(I) (II) (III) (IV)

Model D

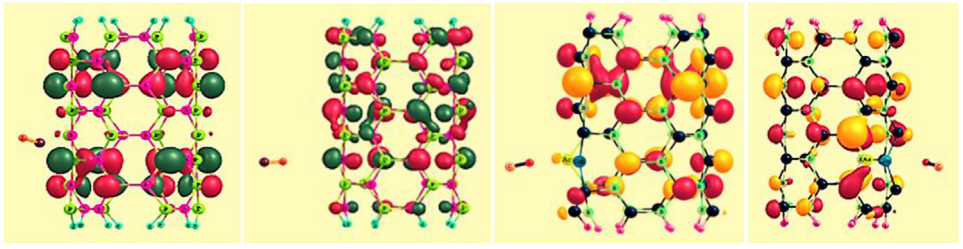

(I) (II) (III) (IV)

Model E

Fig. 3. Plots of HOMO and LUMO structures of CO adsorption on the undoped (models I, II) and the HOMO and LUMO structures of CO adsorption on AsGa-doped (models III, V) of (4, 4) armchair BPNTs, for (A–H) models (see Fig. 2).

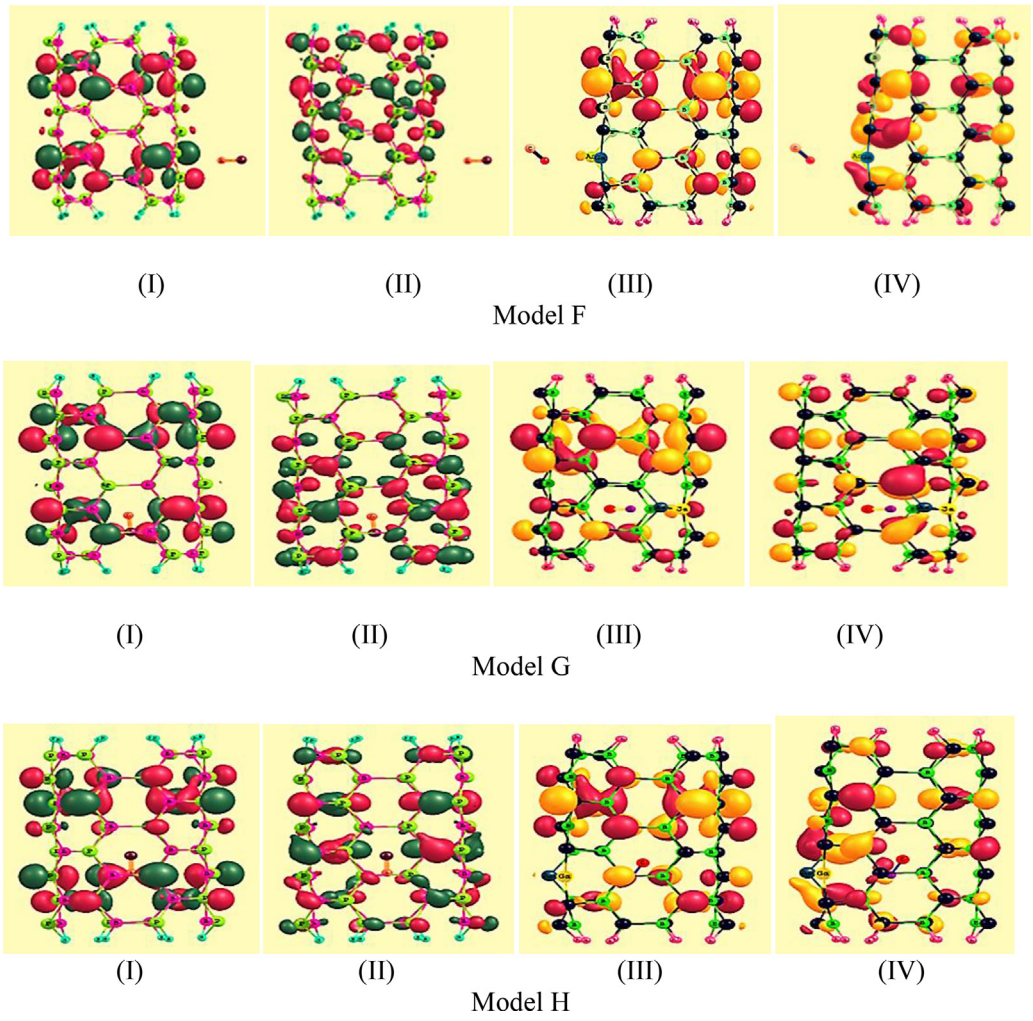

Fig. 3. (*continued*).

Table 3
Quantum parameters for (A-H) models (Figs. 1 and 2) of CO adsorption on pristine and AsGa-doped of (4, 4) armchair models of BNNTs.

	E_{HOMO}/ev	E_{LUMO}/ev	E_{gap}	I/ev	A/ev	μ/ev	S/ev	ω/ev	χ/ev	η/ev
Undoped										
Pristine	−5.863	−2.906	2.957	5.863	2.906	−4.385	0.338	6.502	4.385	1.479
Model (A)	−5.881	−2.864	3.017	5.881	2.864	−4.372	0.331	6.337	4.372	1.508
Model (B)	−5.853	−2.894	2.958	5.853	2.894	−4.373	0.338	6.465	4.373	1.479
Model (C)	−5.857	−2.894	2.963	5.857	2.894	−4.376	0.338	6.462	4.376	1.481
Model (D)	−5.860	−2.897	2.963	5.860	2.897	−4.378	0.338	6.471	4.378	1.481
Model (E)	−5.925	−3.060	2.865	5.925	3.060	−4.493	0.349	7.046	4.493	1.432
Model (F)	−5.925	−3.060	2.865	5.925	3.060	−4.493	0.349	7.046	4.493	1.432
Model (G)	−5.875	−2.906	2.968	5.875	2.906	−4.391	0.337	6.494	4.391	1.484
Model (H)	−5.870	−2.912	2.957	5.870	2.912	−4.391	0.338	6.520	4.391	1.479
AsGa-doped										
Doped	−5.8983	−2.9418	2.957	5.898	2.942	−4.420	0.338	6.608	4.420	1.478
Model (A)	−5.8608	−2.8863	2.975	5.861	2.886	−4.374	0.336	6.431	4.374	1.487
Model (B)	−5.8613	−2.8871	2.974	5.861	2.887	−4.374	0.336	6.433	4.374	1.487
Model (C)	−5.8777	−2.9122	2.966	5.878	2.912	−4.395	0.337	6.513	4.395	1.483
Model (D)	−5.8839	−2.9214	2.963	5.884	2.921	−4.403	0.338	6.543	4.403	1.481
Model (E)	−5.9141	−3.0417	2.872	5.914	3.042	−4.478	0.348	6.981	4.478	1.436
Model (F)	−5.9011	−2.9426	2.958	5.901	2.943	−4.422	0.338	6.609	4.422	1.479
Model (G)	−5.9065	−2.9552	2.951	5.907	2.955	−4.431	0.339	6.652	4.431	1.476
Model (H)	−5.9016	−2.9524	2.949	5.902	2.952	−4.427	0.339	6.645	4.427	1.475

3. Results and discussions

3.1. The structural geometry of CO adsorption on pristine and AsGa-doped

The interaction of CO gas with the (4, 4) armchair BPNTS was investigated by locating the molecule from its O, C head on the center of a hexagonal nanotube. To this aim, several adsorption configurations were applied to determine the most favorable site; each carbon and oxygen atoms of the CO molecule has separately located close to boron and phosphor atom of the nanotube. Eight stable configuration models for CO/BPNTs complexes can be identified (A–H models, see Figs. 1 and 2). Model (A) shows vertical absorption of CO gas on the outer surface of BPNTs via carbon hood; Model (B) indicates vertical absorption of CO gas on the outer surface of BPNTs via oxygen hood; Model (C) shows vertical adsorption of CO gas on inner surface of BPTs via carbon head; Model (D) indicates vertical adsorption of CO gas on inner surface of BPNTs via oxygen head; Model (E) shows parallel adsorption of CO gas on outer surface of BPNTs via carbon head; Model (F) indicates parallel adsorption of CO gas on outer surface of BPNTs via oxygen head; Model (G) shows parallel adsorption of CO gas on inner surface of BPNTs via carbon head; Model (H) indicates parallel adsorption of CO gas on inner surface of BPNTs via oxygen hood. At first step all models are optimized by using the B3LYP level of theory and 6-31G (d) base set, the structural parameters: the bond lengths of (B–P) and bond angles (B–P–B) of the pristine and AsGa-doped of (4, 4) armchair BPNTs are calculated and results tabulated in Table 1. The average B–P bond length of armchair forms of BPNTs is 1.89 Å, which is in agreement with other studies [26–29]. By doping AsGa on the site of the B61 and P62 of (4, 4) armchair form of BPNTs the bond lengths between P51–Ga, P71–Ga, B52–As and B72-As are 2.25, 2.26, 2.02 and 2.02 Å respectively, and by adsorbing CO on the surface of pristine and AsGa-doped BPNTs (Models (A–H)) the bond length changes slightly from the original values. The comparison results reveal that doping of (As and Ga) is a significant effect of a charge transfer from B and P atoms and yielding asymmetric electronic charge density distribution along Ga–p and B–As bonds. On the other hand the adsorption of CO on the surface of BPNTs is slightly affected of a charge transfer from B and P atoms and therefore the bond length is slightly constant. The bond angles of neighbor atoms of AsGa-doped in all models decrease from the original values. The radius of Ga and As is bigger than B and P and therefore doping of As and Ga cause that the neighbor atoms of doping is agglomerated and the bond angles is decreased.

From optimized structures, the adsorption energies (E_{ads}) are calculated by Equation (3), the results of adsorption energy and base set supper position error (BSSE) are given in Table 2. The E_{ads} of the adsorbed CO molecule on the surface of pristine BPNTs has been estimated to be in the range of −4.435–2.272 kcal/mol and for AsGa doped the E_{ads} is in the range −7.003 to −0.653 kcal/mol. These results show that the adsorption of CO on the surface of BPNTs is a physisorption process, which is due to weak Van der Waals interaction between the nanotube and the CO molecule. In addition, the adsorption energies in AsGa-doped BPNTs are always negative and it shows that these processes are exothermic. In comparison the pristine and AsGa-doped models, the results show that, the absolute adsorption energy of the model (A) is more than the absolute adsorption energy of other models.

The calculated adsorption energy for CO in the C–head configuration is higher than that in the O–head, and the boron site was the most stable configuration. When a nanotube is placed under interaction with foreign molecules, its atomic charge distribution is easily changed and the centre of the positive and negative charges of the nanotube change due to redistribution of the atomic charges, consequently leads to the polarization of the nanotube and giving it an induced electric dipole moment.

3.2. Quantum molecular descriptors

For study the distribution of electron density on the surface of nanotube and CO gas at different configuration (A–H) models, we calculate the highest occupied molecular orbital (HOMO) and the lowest unoccupied molecular orbital (LUMO). Plots of HOMOs and LUMOs of CO adsorption on pristine and AsGa-doped of BPNTs (models A–H) are displayed in Fig. 3. The notation (I) and (III) are used for HOMO orbitals of pristine and AsGa-doped of BPNTs respectively, and (II) and (IV) are used for LUMO orbitals of pristine and AsGa-doped of BPNTs respectively. The comparison results reveal that by adsorbing CO at (A–H) models the most density of HOMO orbital for pristine and AsGa-doped of BPNTs is localized on the layers 2, 3 and 4. Meanwhile the most density of LUMO orbitals for the pristine and AsGa-doped of BPNTs are localized on neighbor of CO adsorption sites. Due to acceptor effects of CO the electron charge density around adsorption sites decrease.

The quantum molecular descriptors for (A–H) models of adsorbed CO on surface of pristine and AsGa-doped models of BPNTs are calculated by Equations (4)–(9) and results are summarized in Table 3. The values of differences between HOMO and LUMO energies, band gap energies, in the optimized structures yielded 2.95 eV for the pristine model of BPNTs and by doping AsGa atoms the band gap is constant. On the other hand by adsorbing CO at different configurations (A–H) models the band gap energy slightly changes. This trend revealed that by doping AsGa and adsorbing CO on the surface of BPNTS the conductivity of CO/BPNTs

Table 4
NQR parameters of CO adsorption on pristine and AsGa-doped (4,4) armchair BPNTs at models (A–H) (see Figs. 1 and 2).

Nucleus	Pristine		Model(A)		Model(B)		Model(C)		Model(D)		Model(E)		Model(F)		Model(G)		Model(H)	
	$C_{Q/MHz}$	η_Q	$C_{Q/MHz}$	η_Q	$C_{Q/MHz}$	η_Q	$C_{Q/MHz}$	η_Q	$C_{Q/MHz}$	η_Q	$C_{Q/MHz}$	η_Q	$C_{Q/MHz}$	η_Q	$C_{Q/MHz}$	η_Q	$C_{Q/MHz}$	η_Q
Undoped																		
Layer 1	3.94	0.30	3.94	0.29	3.94	0.30	3.94	0.30	3.94	0.30	3.94	0.30	3.94	0.30	3.94	0.30	3.94	0.30
Layer 2	2.57	0.08	2.57	0.08	2.58	0.08	2.58	0.08	2.58	0.08	2.58	0.08	2.58	0.08	2.58	0.08	2.59	0.08
Layer 3	2.52	0.11	2.52	0.12	2.51	0.11	2.52	0.11	2.51	0.11	2.52	0.12	2.52	0.12	2.51	0.11	2.51	0.12
Layer 4	2.39	0.07	2.44	0.08	2.39	0.07	2.40	0.07	2.39	0.07	2.42	0.08	2.42	0.08	2.39	0.07	2.40	0.07
Average	2.85	0.14	2.80	0.15	2.85	0.14	2.86	0.14	2.85	0.14	2.84	0.16	2.84	0.16	2.86	0.14	2.86	0.14
AsGa-doped																		
Layer 1	3.94	0.30	3.94	0.30	3.94	0.30	3.94	0.30	3.94	0.30	3.94	0.30	3.94	0.30	3.94	0.30	3.94	0.30
Layer 2	2.57	0.08	2.57	0.08	2.57	0.08	2.58	0.08	2.58	0.08	2.58	0.08	2.58	0.08	2.58	0.08	2.58	0.08
Layer 3	2.51	0.11	2.51	0.11	2.51	0.11	2.51	0.11	2.51	0.11	2.51	0.11	2.51	0.11	2.51	0.11	2.51	0.11
Layer 4	2.41	0.07	2.41	0.07	2.41	0.07	2.41	0.07	2.41	0.07	2.43	0.08	2.42	0.08	2.42	0.08	2.43	0.08
Average	2.85	0.14	2.85	0.14	2.85	0.14	2.85	0.14	2.85	0.14	2.87	0.15	2.85	0.14	2.86	0.14	2.85	0.14

complex is slightly changed. The electronic chemical potential is a measure of the tendency of electrons to escape a system and can be related to the energies of the HOMOs and LUMOs via Koopman's theorem [39], where (I) is the ionization potential and A is the electron affinity [40,41]. Due to the average local ionization energy ($\bar{I}$) was introduced as a means for identifying reactive sites on surface including nanotubes, ($\bar{I}$) has been connected to electronegativity, local polarizability and hardness. These characteristics

Fig. 4. Plots of CSI *vs.* B and P sites of (I) pristine and AsGa-doped model of BPNTs and (II) (A–H) model of adsorption CO on pristine and AsGa-doped of BPNTs.

are discussed in detail elsewhere [42]. The μ is also equal to the negative of Mulliken's electronegativity: the average of I and A [43,44]. The average values of chemical potential (μ) electrophilicity index (ω) and the global hardness (η) for all (A-H) pristine and AsGa-doped is − 4.372, 6.460 and 1.481 eV respectively and by doping AsGa and adsorbing CO all values slightly change.

3.3. NQR parameters of ^{11}B

From optimized structures of CO adsorption on pristine and AsGa doped of BPNTs models (A–H), the NQR parameters of ^{11}B nuclei at different sites are calculated by Equations (9 and 10) and results are tabulated in Table 4. The NQR parameters of 32 B atoms in all considered models of the (4, 4) armchair are separated into four layers based on the similarity of the calculated electric field gradient (EFG) tensors in each layer; therefore, the electrostatic environment of the BPNTs is equivalent along each layer. Comparison results show that the CQ values of the first layer at all models are the largest among other layers (Table 4). The results show that the orientation of the EFG tensor eigenvalues along the z-axis of the first layer is stronger than the other layers along the length of the nanotube. On the other hand the fourth layer has the low C_Q among of other layers in alone nanotube. The significant difference between NQR parameters in the first layer and the fourth layer is due to the change of the geometrical parameters. By adsorbing of CO gas the C_Q values of the four layers of models (A–H) undoped and AsGa doped models remain almost unchanged. Therefore the electric field gradient (EFG) tensors in each layer by adsorption of CO and doping of AsGa are constant.

3.4. The NMR parameters of adsorption of CO on BPNTs

The NMR (CSI and CSA) parameters of ^{11}B nuclei and ^{31}P nuclei for adsorption of CO on the pristine and AsGa-doped models (4, 4) armchair BPNTs (Figs. 1 and 2) are calculated by Equations (1) and (2) and the evaluated NMR parameters are presented in Supplementary data. A look at the results for the pristine (4, 4) armchair BPNTs show that various ^{11}B and ^{31}P nuclei are divided into four layers with equivalent calculated CSI and CSA parameters, which means that the nuclei in each layer have equivalent electrostatic properties. The direction of the changes for isotropic and anisotropic chemical shielding because of differences in physical concept of these parameters is different. The CSI values for B nuclei in the end layer are bigger than other layers, meaning boron nuclei in this layer have maximum electron shielding, but in the first layer of nanotubes is minimized. The plot of CSI values of pristine and (A-H) adsorption models for ^{11}B and ^{31}P nuclei are shown in Fig. 4. The results of b-II Fig. 4 shows that by adsorbing CO at the models A, B, C and D CSI values of B61 sites increase significantly from unabsorbed and other models. In these models adsorption of CO on the vertical direction of nanotube increase the electron density around B61 site and so the CSI tensors at this site increase. Meanwhile the CSI values of the P51 and P62b sites (plot d-II, Fig. 4) models A, B, C and D increase significantly from original values and other models is slightly constant. It is notable that by doping AsGa the CSI values at sites B42 and B62 of unabsorbed model (plot e-I) increase significantly from pristine models due to donor electron effects of As and Ga doped. By adsorbing CO at all models (plot f-II) the CSI values of sites B42 and B62 is bigger than other sites and on the other hand, at the models B, E, F and H the CSI values of the site B71 increase significantly from unabsorbed model therefore at set B71 the effect of CO adsorption is more notable than other sites. The comparison of CSI values for ^{31}P pristine and AsGa-doped (plot c-I and g-I) show that by doping AsGa the CSI values at sites P51 and P62 increase more significantly than undoped models. It is notable that by adsorbing CO the CSI values of sites P51 and P62 at F, G, H models decrease significantly than other models. In these models adsorption CO at horizontal direction on surface decrease the electron density at P51 and P62 sites and so decrease the CSI vales tensors.

4. Conclusions

In this work, we studied the effects of AsGa-doped on the adsorption of CO on the outside and inside surface of (4, 4) armchair BPNTs by using the density functional theory (DFT) calculations, as well as structural and electronic properties including bond lengths, bond angles, energy gaps, molecular orbital energies, adsorption energy, NQR parameters, NMR parameters and quantum molecular descriptors. The calculated adsorption energy for CO in the C–head configuration is higher than that in the O–head, and the boron site was the most stable configuration. We also showed that when the complex is exposed to an external electric field, it has a much stronger interaction with the electrodes of the nanoelectronic circuit. Our results suggest that the AsGa-doped BPNTs are more favorable than pristine models for CO adsorption. In addition, the CO adsorption decreases the band gap of the pristine BPNTs, and increases their electrical conductance. The global hardness and ionization potential because of CO adsorption decrease of original value. The C_Q parameter of the first layer of all models is larger than the other layers. Meanwhile doping AsGa and adsorption CO increase the CSI values at sites of B42, B62, P51 and P62 of BPNTs due to donor electron effects of CO and AsGa-doped.

Acknowledgment

The authors thank the Centre of computational Nano of Malayer Universities for supporting this research.

Appendix A. Supplementary data

Supplementary data related to this article can be found at http://dx.doi.org/10.1016/j.cocom.2015.01.001.

References

[1] Y. Xie, Y.P. Huob, J.M. Zhang, Appl. Surf. Sci. 258 (2012) 6391.
[2] R. Wang, D. Zhang, W. Sun, Z. Han, C. Liu, J. Mol. Struct. (THEOCHEM) 806 (2007) 93.
[3] J.X. Zhao, Y.H. Dinga, Mater. Chem. Phys. 110 (2008) 411.
[4] C. Zhi, Y. Bando, C. Tan, D. Golberg, Solid State Commun. 135 (2005) 67.
[5] T. Oku, N. Koi, K. Suganuma, Diam. Relat. Mater. 17 (2008) 1805.
[6] D. Golberg, Y. Bando, T. Sato, J. Nanosci. Nanotechnol. 44 (2001) 1561.
[7] M. Hamadanian, B. Khoshnevisan, F. Kalantari Fotooh, Z. Tavangar, Comput. Mater. Sci. 58 (2012) 45.
[8] J. Beheshtian, A. Ahmadi Peyghan, Z. Bagheri, Comput. Mater. Sci. 62 (2012) 71.
[9] K. Fukui, M. Nakane, Sens. Actuators B. Chem. 24 (1995) 486.
[10] S. Zhuiykov, W. Wlodarski, Y. Li, Sens. Actuators B Chem. 77 (2001) 484.
[11] H. Chang, J. Lee, S. Lee, Y. Lee, Appl. Phys. Lett. 79 (2001) 3863.
[12] J. Lu, S. Nagase, Y. Maeda, T. Wakahara, T. Nakahodo, T. Akasaka, D. Yu, Z. Gao, R. Han, H. Ye, Chem. Phys. Lett. 405 (2005) 90.
[13] S. Santucci, S. Picozzi, F. Di Gregorio, L. Lozzi, C. Cantalini, L. Valentini, J.M. Kenny, B. Delley, J. Chem. Phys. 119 (2003) 10904.
[14] Z. Zanolli, J.C. Charlier, Phys. Rev. B 80 (2009) 155447.
[15] K. Azizi, S. Majid Hashemianzadeh, S.H. Bahramifar, Curr. Appl. Phys. 11 (2011) 776.
[16] P.A. Denis, Chem. Phys. 353 (2008) 79.
[17] C.S. Yeung, L.V. Liu, Y.A. Wang, J. Phys. Chem. C 112 (2008) 7401.
[18] M.T. Beheshtian, M.T. Baei, A.A. Peyghan, Surf. Sci. 606 (2012) 981.
[19] A.A. Peyghan, A. Soltani, A.A. Pahlevani, Y. Kanani, S. Khajeh, Appl. Surf. Sci. 270 (2013) 25–32.
[20] Y. Kanani, M.T. Baei, A. Varasteh Moradi, A. Soltani, Phys. E 59 (2014) 66–74.
[21] J.X. Zhao, Y.H. Ding, Mater. Chem. Phys. 110 (2008) 411.
[22] W. An, X. Wu, J.L. Yang, X.C. Zeng, J. Phys. Chem. C 111 (2007) 14105.
[23] R.Q. Wu, M. Yang, Y.H. Lu, Y.P. Feng, Z.G. Huang, Q.Y. Wu, J. Phys. Chem. C 112 (2008) 15985.
[24] J. Beheshtian, Z. Bagheri, M. Kamfiroozi, A. Ahmadi, Struct. Chem. 23 (2012)

653.
[25] W. An, C.H. Turner, Chem. Phys. Lett. 482 (2009) 274.
[26] M. Rezaei-Sameti, Phys. E 43 (2010) 588.
[27] M. Rezaei-Sameti, Phys. B 407 (2012) 3717.
[28] M. Rezaei-Sameti, Phys. B 407 (2012) 22.
[29] M. Rezaei-Sameti, Phys. E 44 (2012) 1770.
[30] M.J. Frisch, et al., GAUSSIAN 03 (2003).
[31] R. Ditchfield, W.J. Hehre, J.A. Pople, J. Chem. Phys. 54 (1972) 724.
[32] M.T. Baei, M. Moghimi, P. Torabi, A. Varasteh Moradi, Comput. Theor. Chem. 972 (2011) 14.
[33] P.K. Chattaraj, U. Sarkar, D.R. Roy, Chem. Rev. 106 (2006) 2065.
[34] K.K. Hazarika, N.C. Baruah, R.C. Deka, Struct. Chem. 20 (2009) 1079.
[35] R.G. Parr, L. Szentpaly, S. Liu, J. Am. Chem. Soc. 121 (1999) 1922.
[36] R.G. Pearson, J. Chem. Sci. 111 (2005) 369.
[37] B.C. Gerstein, C.R. Dybowski, Transient Techniques in NMR of Solids, Academic Press, New York, 1985.
[38] P. Pyykkö, Mol. Phys. 99 (2001) 1617.
[39] T. Koopmans, Physica 1 (1993) 104.
[40] R.G. Pearson, J. Am. Chem. Soc. 85 (1963) 3533.
[41] R.G. Parr, R.G. Pearson, J. Am. Chem. Soc. 105 (1983) 7512.
[42] P. Politzer, J.S. Murray, F.A. Bulat, J. Mol. Model. 16 (2010) 1731.
[43] R.S. Mulliken, J. Chem. Phys. 2 (1934) 782–793.
[44] C. Tabtimsai, S. Keawwangchai, N. Nunthaboot, V. Ruangpornvisuti, B. Wanno, J. Mol. Model. 18 (2012) 3941.